中国科学院国家天文台
National Astronomical Observatories, CAS

the SILK ROAD PROJECT at NAOC
丝绸之路 计划

RECRUITMENT PROGRAM OF GLOBAL EXPERTS

Pulsar Timing, gravitational waves, Supermassive black holes

Rainer Spurzem* + Silk Road Project Team
National Astronomical Observatories (NAOC), Chinese Academy of Sciences
Kavli Institute for Astronomy and Astrophysics (KIAA), Peking University
Max-Planck Inst. for Astronomy, Garching/Munich, Germany
Astronomisches Rechen-Inst., ZAH, Univ. of Heidelberg, Germany

spurzem@nao.cas.cn
http://silkroad.bao.ac.cn
*Special State Foreign Expert in Thousand People's Plan in China

Deutsche Forschungsgemeinschaft SFB881 DFG

国家自然科学基金委员会 National Natural Science Foundation of China

NVIDIA World Leader in Visual Computing Technologies

EGO EUROPEAN GRAVITATIONAL OBSERVATORY

VolkswagenStiftung

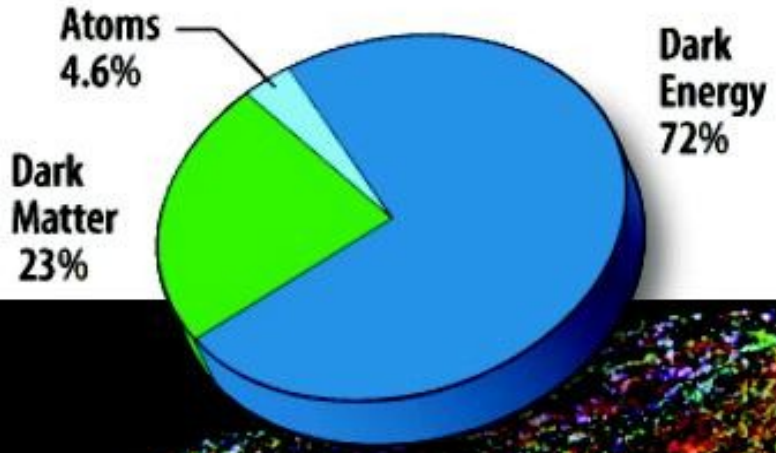

WMAP

2.725 Kelvin

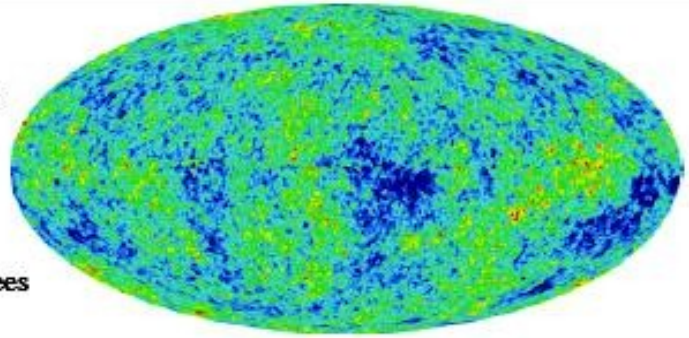

0.0002 degrees

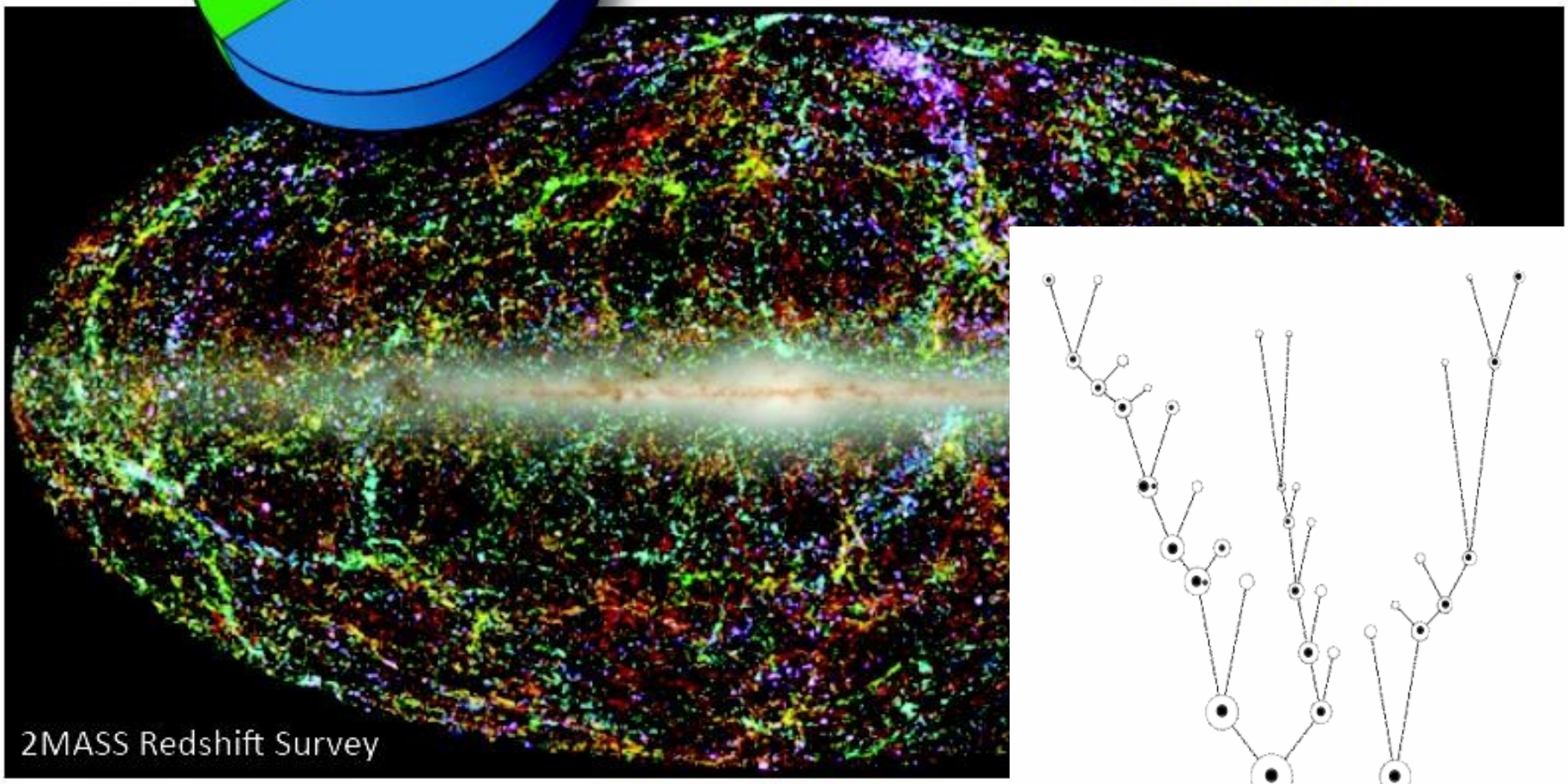

(Image: T.H. Jarrett (IPAC/SSC))

Simulations of Binary Black Holes

Black Holes in Dense Stellar Clusters:
N-Body Problem with General Relativity (Post-Newtonian)

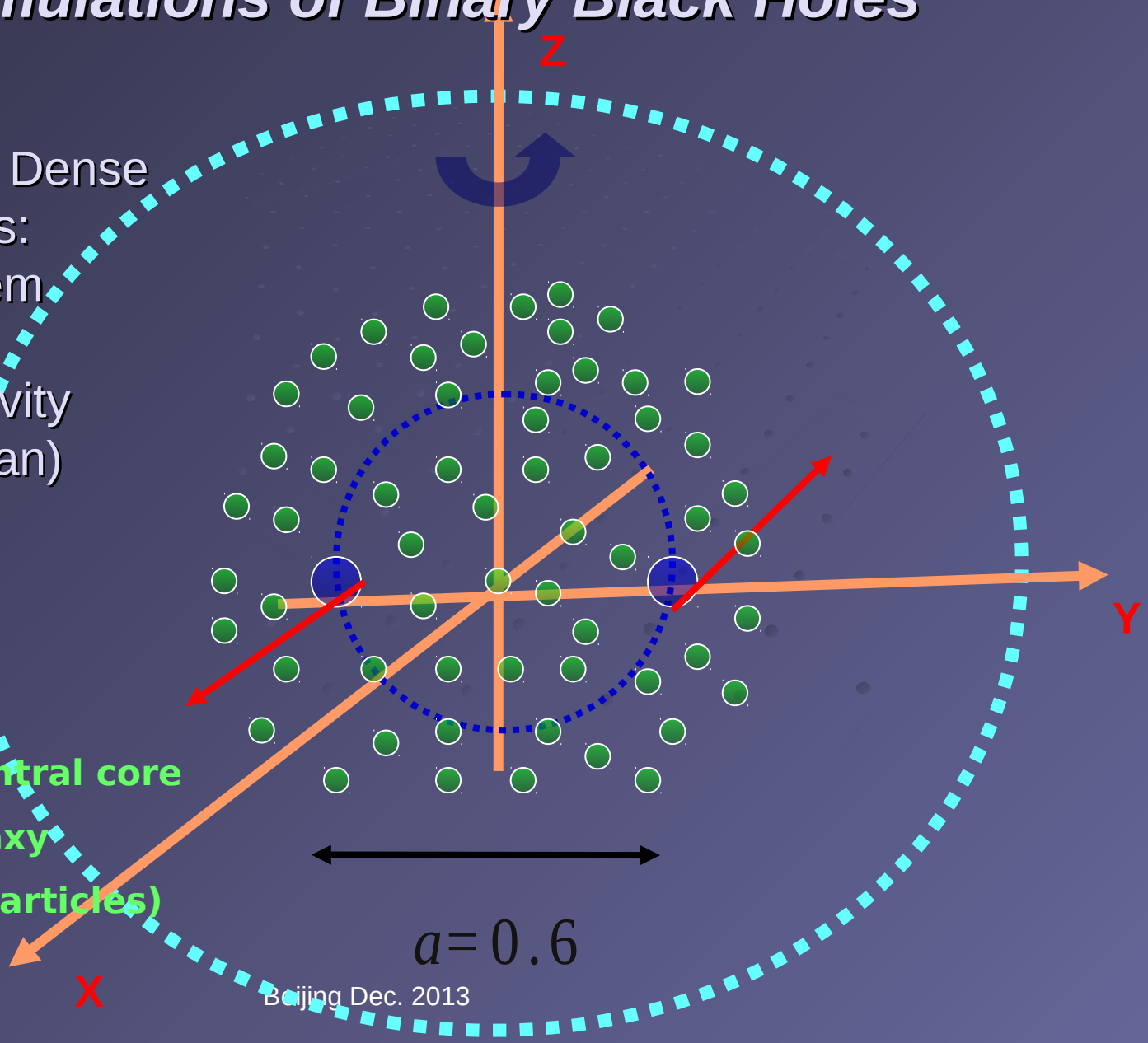

Two equal-mass black holes in central core of simplified galaxy (up to 4 million particles)

Dynamics of Binary Black Holes in Galactic Nuclei

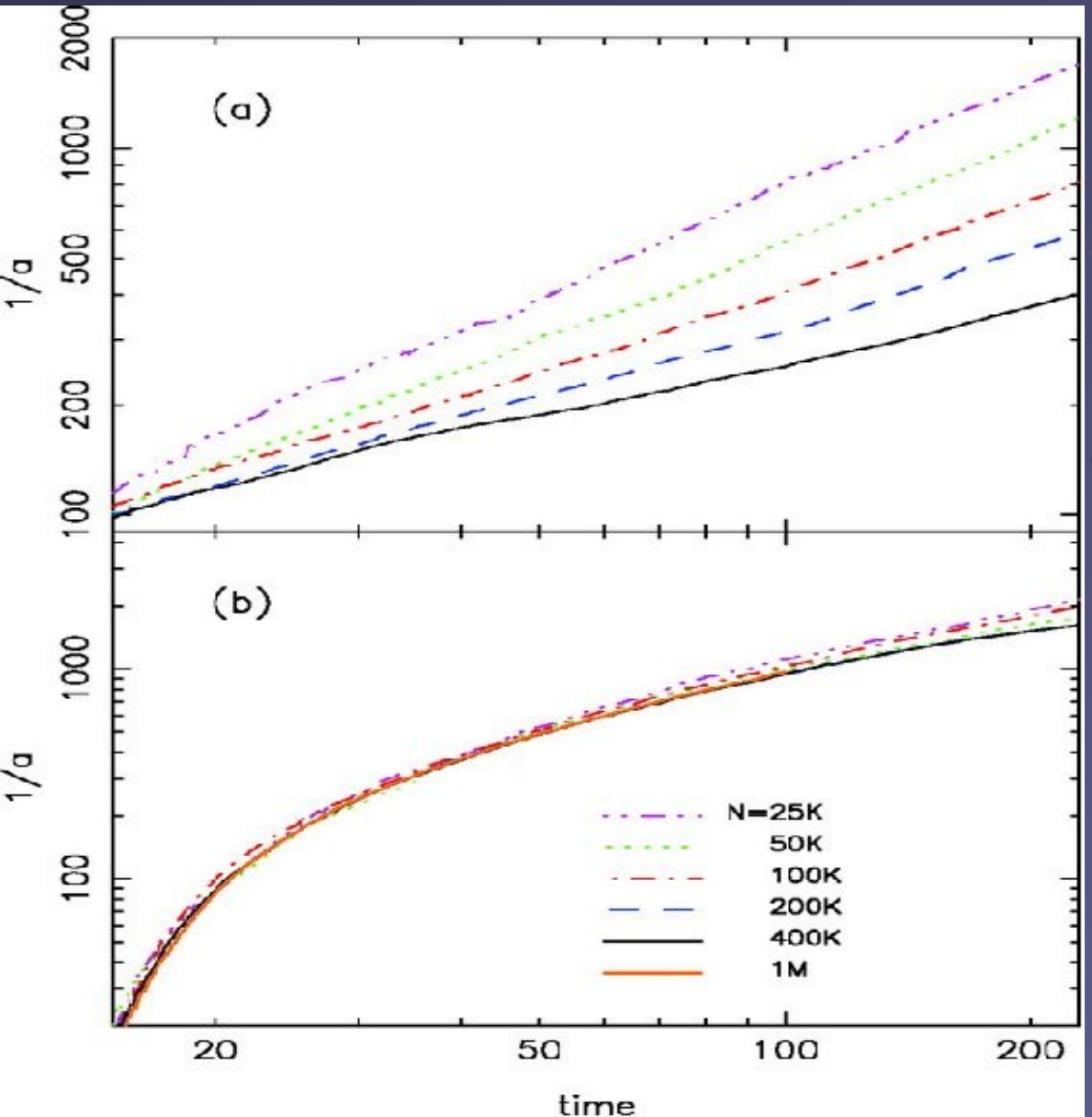

Spherical Systems:
BH binary stalls with N

Axisymmetric,
Rotating systems:
No stalling observed

Berczik, Merritt, Spurzem, 2005, ApJ
Berczik, Merritt, Spurzem, Bischof, 2006, ApJ
Berentzen, Preto, Berczik, Merritt, Spurzem, 2009, ApJ
Fiestas & Spurzem, 2010,11 MNRAS
Amaro-Seoane, ..., Sp, MNRAS 2010
Preto, Berentzen, Berczik, Spurzem et al. 2011
Khan et al. 2011a, b

Merging of two “Galaxies” (Dehnen Models with Black Hole)

Preto, Berczik, Berentzen, Spurzem, 2011, ApJ

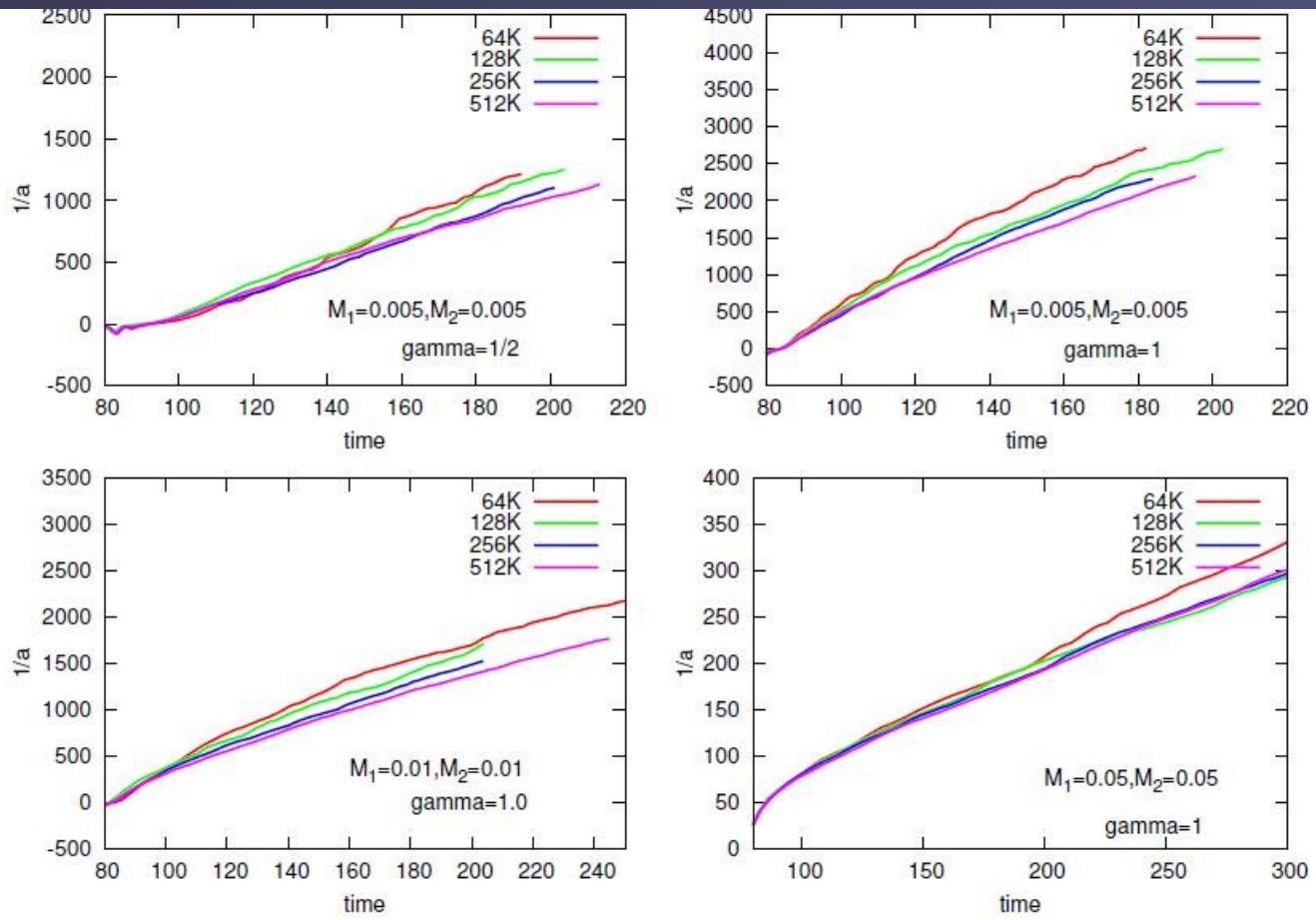

Figure 2: Hardening rate, *i.e*, the rate at which the inverse semimajor axis $1/a$ increases during the MBHB inspiral after the two nuclei have merged and the MBH have formed a bound pair. The four panels correspond to runs with equal mass binaries ($q = 1$), each with a different total mass $M_{12} = M_1 + M_2$. Gamma ($\equiv \gamma$) stands for the initial central stellar density slope around the MBH in each nucleus before they merge. The hardening rates converge for particle number as low as $N = 128K$. [taken from [3]]

Dynamics of Supermassive Single and Binary Black Holes in Galactic Nuclei

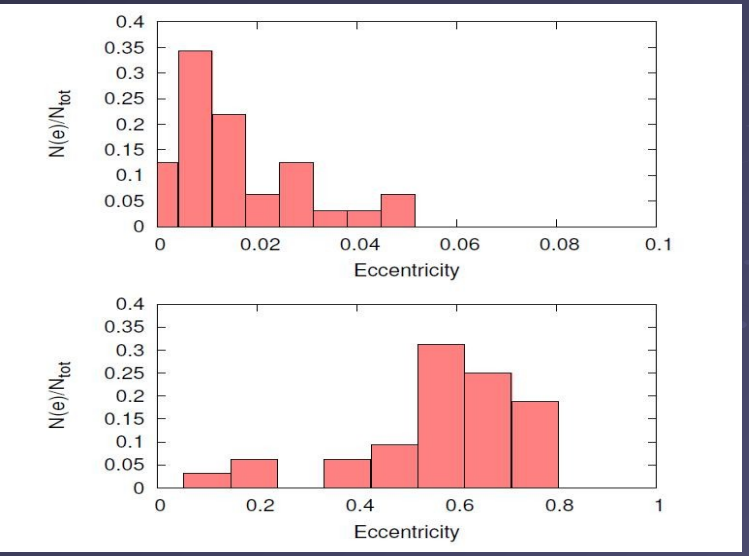

Eccentricity Matters

-

Preto, Berentzen, Berczik, Spurzem, 2011, ApJ
Khan, Berentzen, Berczik, Just, Mayer, Nitadori, Callegari, 2012, ApJ

Figure below, from Just, ... Berczik, Spurzem, ..., 2012, ApJ

The presence of an accretion disk near an SMBH enhances the mass growth rate of SMBH by factor 3.

Figure on top: lower panel: eccentricity when supermassive binary black hole (SMBH) becomes bound. Upper panel: eccentricity shortly before Final relativistic merger. This is important to predict gravitational waveforms correctly.

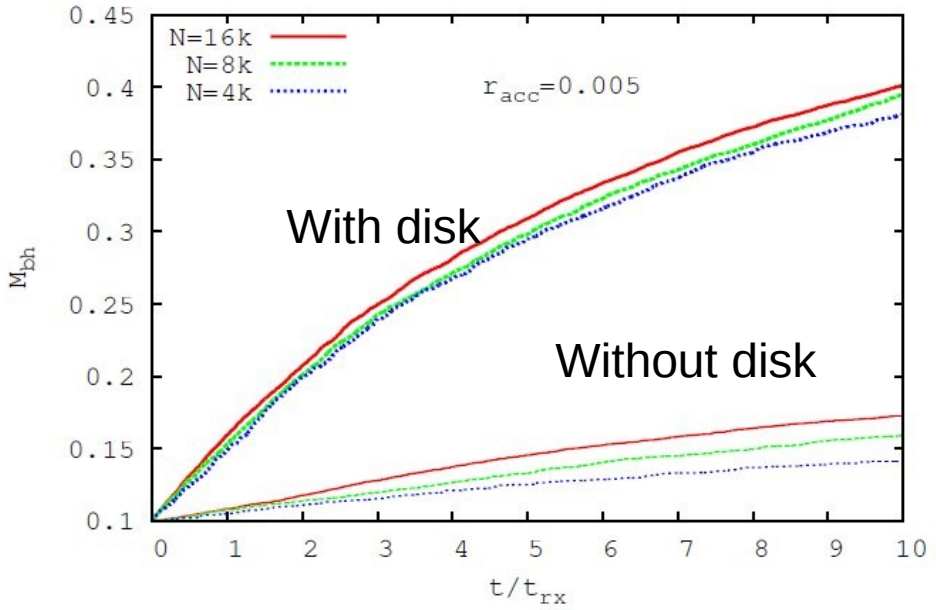

Dynamics of Binary Black Holes in Galactic Nuclei

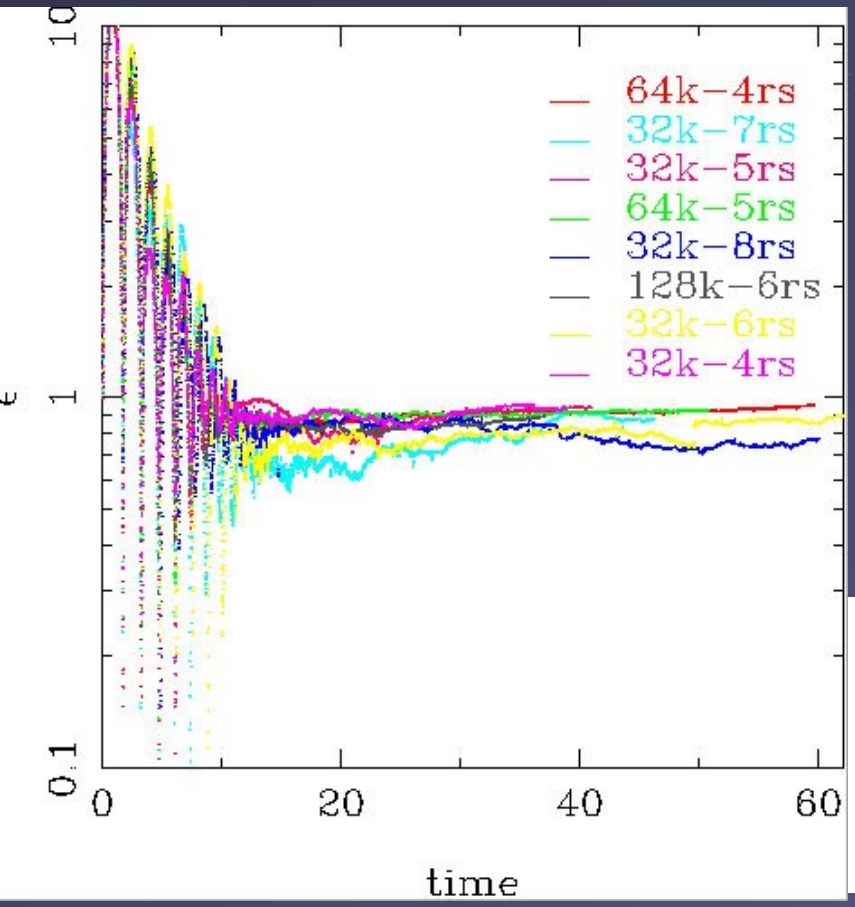

- Hemsendorf, Sigurdsson, Spurzem, 2002 , Astroph. Jl.
- Cf. also Aarseth & Mikkola (2003), Funato & Makino (2005), Makino et al. 1993, ...
- High Eccentricity if loss cone full!

Time Scale for GR merger: $t_{GR} \propto M^{-3}(1-e^2)^{7/2}$

Important for Background of Ultra-Low GR frequencies (LISA!) 0.01-1 μHz

Post-Newtonian Dynamics

Two approaches: 1. Quasi-Newtonian Source
compute far-field grav. radiation,
Einstein quadrupole formula, Landau-Lifschitz.
from energy loss compute orbital change

$$h_{ij}^{\rm TT} = \frac{2G}{c^4 R}\mathcal{P}_{ijab}(\mathbf{N})\left\{\frac{d^2\mathrm{Q}_{ab}}{dT^2}(T-R/c)+\mathcal{O}\left(\frac{1}{c}\right)\right\}+\mathcal{O}\left(\frac{1}{R^2}\right), \tag{2}$$

where $R = |\mathbf{X}|$ is the distance to the source, $\mathbf{N} = \mathbf{X}/R$ is the unit direction from the source to the observer, and $\mathcal{P}_{ijab} = \mathcal{P}_{ia}\mathcal{P}_{jb} - \frac{1}{2}\delta_{ij}\mathcal{P}_{ij}\mathcal{P}_{ab}$ is the TT projection operator, with $\mathcal{P}_{ij} = \delta_{ij} - N_i N_j$ being the projector onto the plane orthogonal to $\mathbf{N}$. The source's quadrupole moment takes the familiar Newtonian form

$$\mathrm{Q}_{ij}(t) = \int_{\rm source} d^3\mathbf{x}\,\rho(\mathbf{x},t)\left(x_i x_j - \frac{1}{3}\delta_{ij}\mathbf{x}^2\right), \tag{3}$$

where ρ is the Newtonian mass density. The total gravitational power emitted by the source in all directions is given by the Einstein quadrupole formula

$$\mathcal{L} = \frac{G}{5c^5}\left\{\frac{d^3\mathrm{Q}_{ab}}{dT^3}\frac{d^3\mathrm{Q}_{ab}}{dT^3}+\mathcal{O}\left(\frac{1}{c^2}\right)\right\}. \tag{4}$$

Pioneers: Peters & Mathews 1963, Peters 1964 Tyson & Giffard 1978

What happens? Use Post-Newtonian approximation...

(G. Schäfer, A. Gopakumar et al.)

$$\mathcal{H}(\mathbf{r},\hat{\mathbf{p}}) = \mathcal{H}_0(\mathbf{r},\hat{\mathbf{p}}) + \frac{1}{c^2}\mathcal{H}_1(\mathbf{r},\hat{\mathbf{p}}) + \frac{1}{c^4}\mathcal{H}_2(\mathbf{r},\hat{\mathbf{p}}) + \frac{1}{c^6}\mathcal{H}_3(\mathbf{r},\hat{\mathbf{p}}),$$

Hamiltonian

particle acceleration (Lagrangian)

- Conservative (Hamiltonian) Terms, so-called PN 1,2,3.... (Perihel Shifts)
- Dissipative Terms PN 2.5, 3.5 (Emission of Energy in gravitational waves, emission of linear momentum in unequal mass case!)
- Spin-Spin, Spin-Orbit-Couplings PN 1.0 + x …!

Schäfer, Gauge Theor. Grav. 36, 2223 (2004)
Memmesheimer, Gopakumar, Schäfer, Phys. Rev.D 70, 104011 (2004)

We use now: PN1 PN2 PN2.5

Post-Newtonian Dynamics

Method A: use geodetic equations, harmonic gauge, directly obtain eqs. of motion (Blanchet et al.)

Method B: Hamiltonian approach using ADM gauge (Schaefer et al.)

A and B equivalent till PN2.5 (1/c**5), higher order gauge functions appear.

$$\frac{dv^i}{dt} = -\frac{Gm}{r^2}\left[(1+\mathcal{A})\,n^i + \mathcal{B}\,v^i\right] + \mathcal{O}\left(\frac{1}{c^8}\right), \tag{181}$$

and find [43] that the coefficients $\mathcal{A}$ and $\mathcal{B}$ are

$$\mathcal{A} = \frac{1}{c^2}\left\{-\frac{3\dot{r}^2\nu}{2} + v^2 + 3\nu v^2 - \frac{Gm}{r}(4+2\nu)\right\}$$

Perihel shift

$$+\frac{1}{c^4}\left\{\frac{15\dot{r}^4\nu}{8} - \frac{45\dot{r}^4\nu^2}{8} - \frac{9\dot{r}^2\nu v^2}{2} + 6\dot{r}^2\nu^2v^2 + 3\nu v^4 - 4\nu^2v^4\right.$$

... higher order...

$$\left. + \frac{Gm}{r}\left(-2\dot{r}^2 - 25\dot{r}^2\nu - 2\dot{r}^2\nu^2 - \frac{13\nu v^2}{2} + 2\nu^2v^2\right) + \frac{G^2m^2}{r^2}\left(9 + \frac{87\nu}{4}\right)\right\}$$

$$+\frac{1}{c^5}\left\{-\frac{24\dot{r}\nu v^2}{5}\frac{Gm}{r} - \frac{136\dot{r}\nu}{15}\frac{G^2m^2}{r^2}\right\}$$

Grav. Radiation

Post-Newtonian Dynamics

What happens afterwards? Post-Newton Order „2.5“...

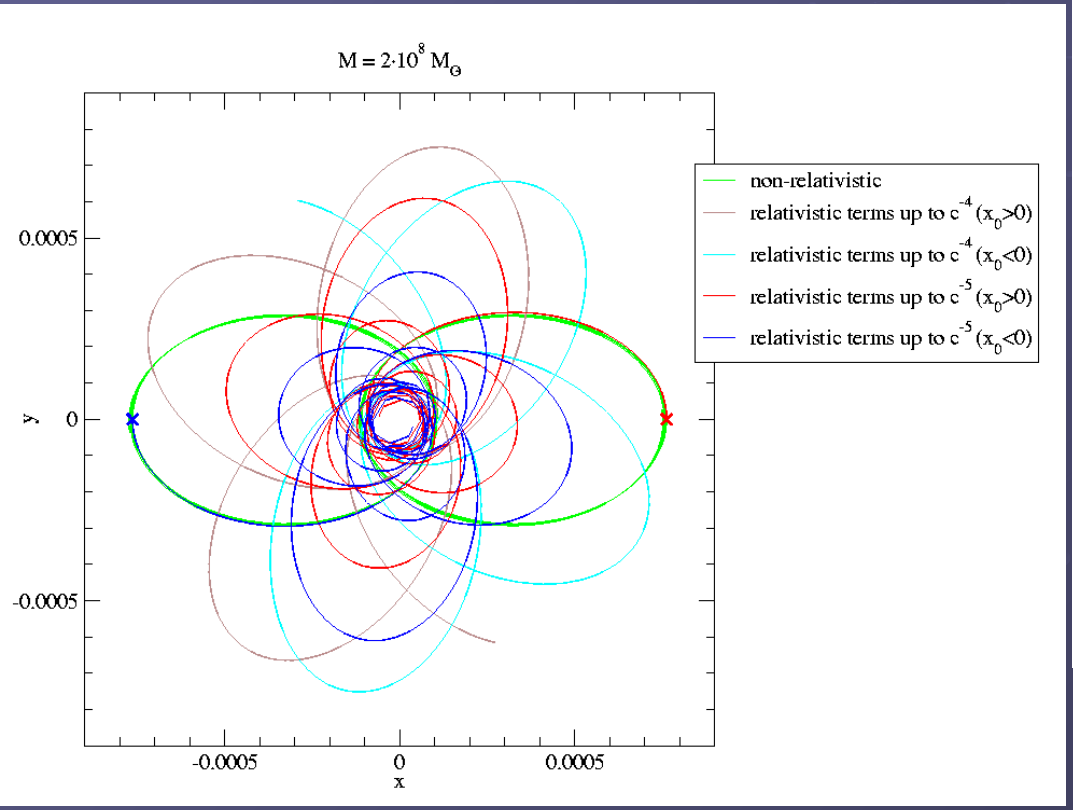

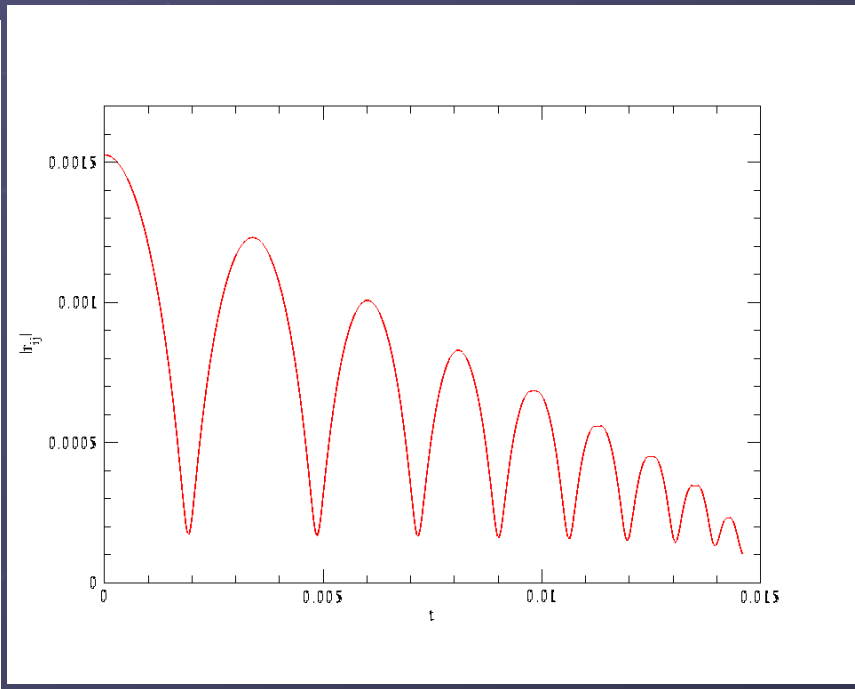

Kupi, Amaro-Seoane & Spurzem 2006

Post-Newtonian Dynamics... and they merge!

$$f[\mathrm{Hz}] = f_0\, 10^{-13}\, (1/a)^{(-3/2)}$$

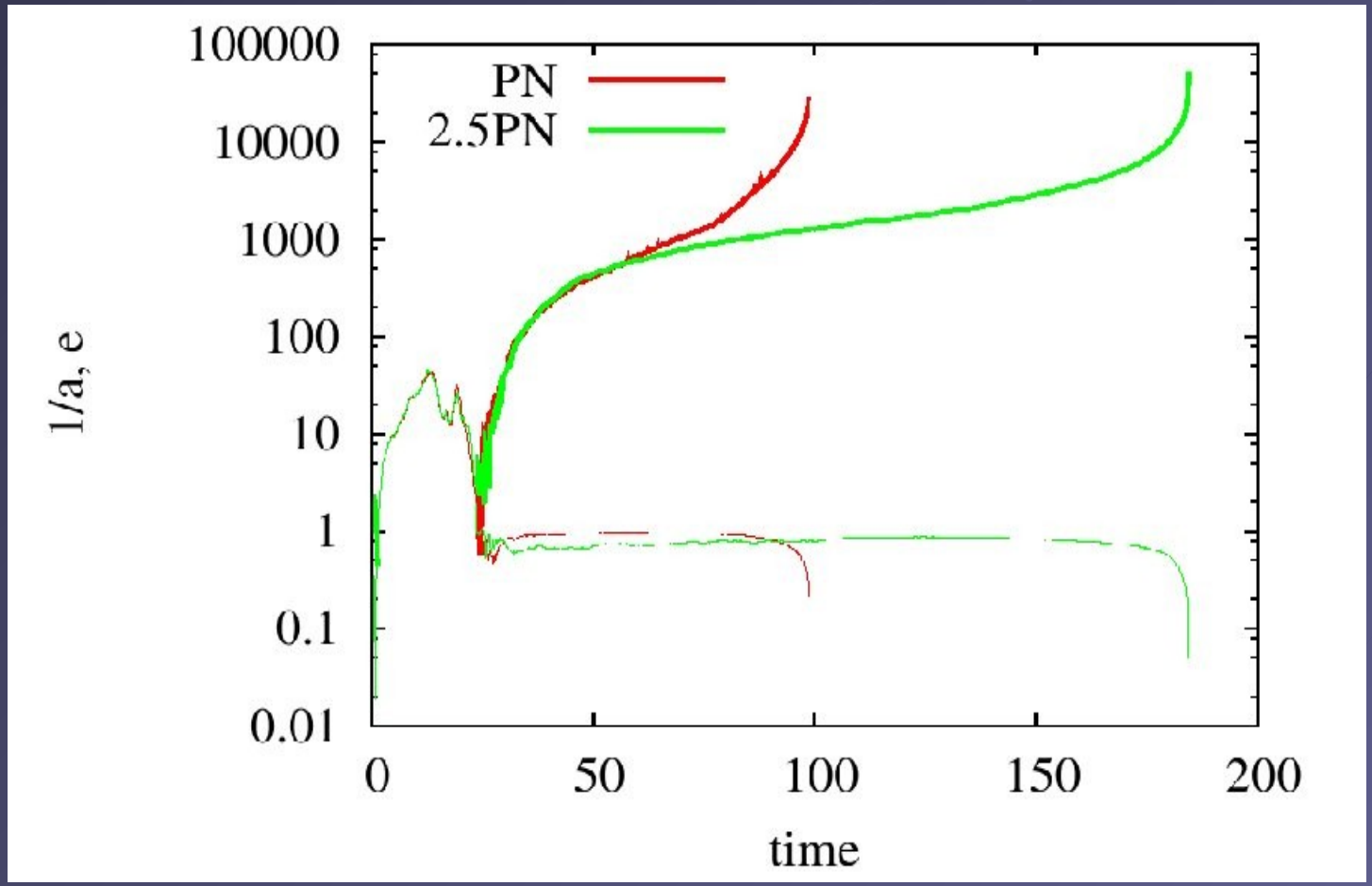

Berentzen, Preto, Berczik, Merritt, Spurzem, 2009, ApJ

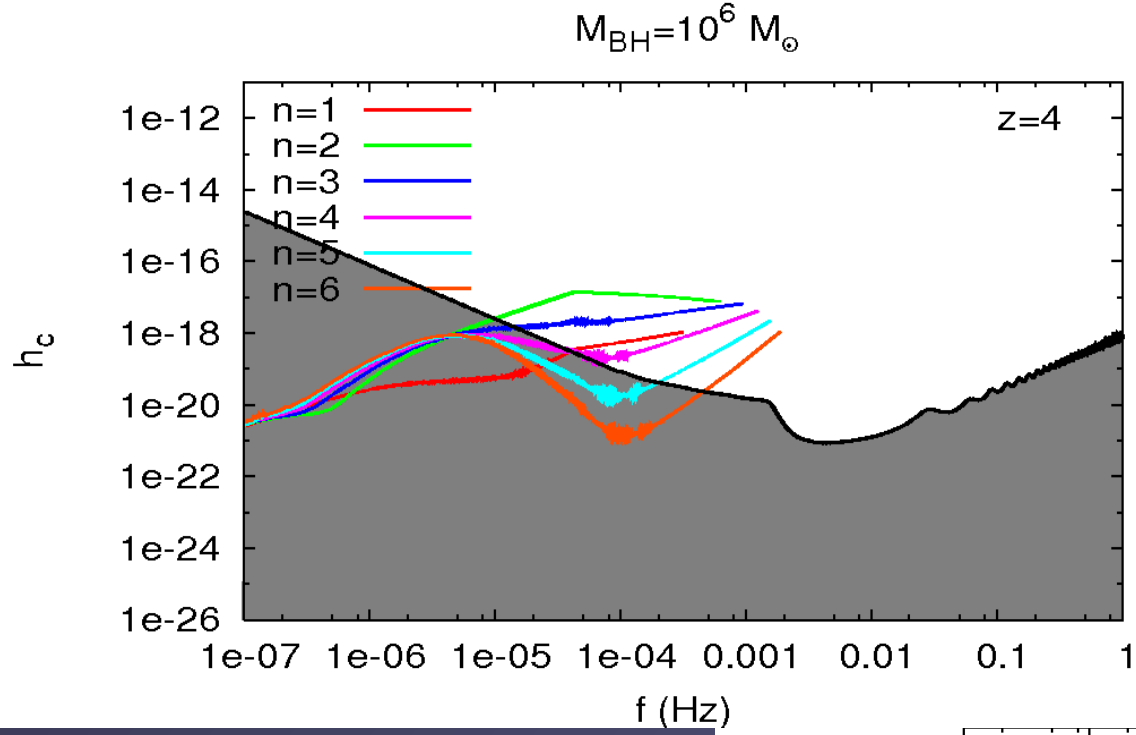

Berentzen, Preto, Berczik, Merritt, Spurzem
2009 (ApJ)

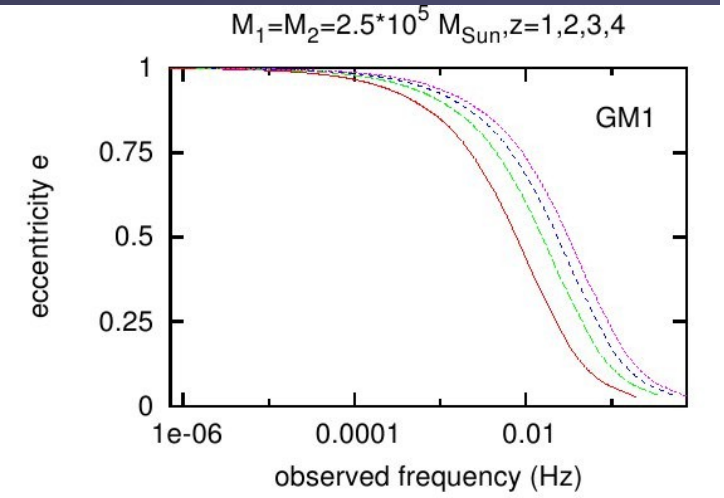

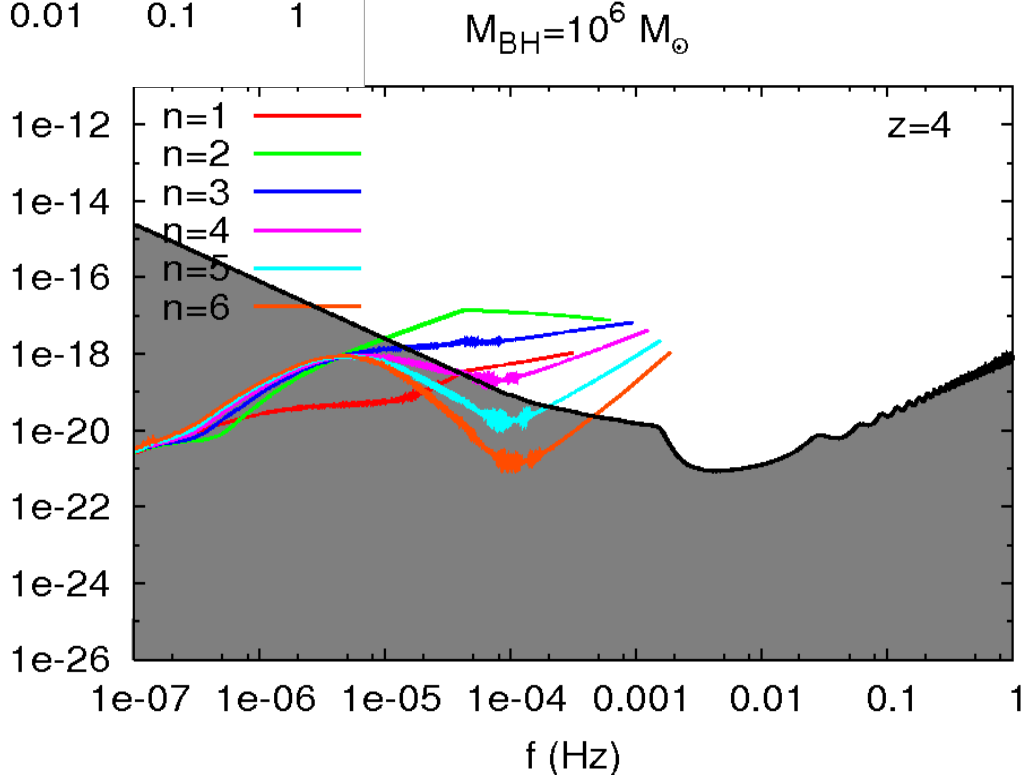

Post-Newtonian Dynamics

Comparison of Post-Newtonian and Newtonian Perturbative Forces with Two-Body Newtonian...

Preto, Berentzen, Berczik, Merritt, Spurzem 2009,
7th LISA-Symposium, JPhCS

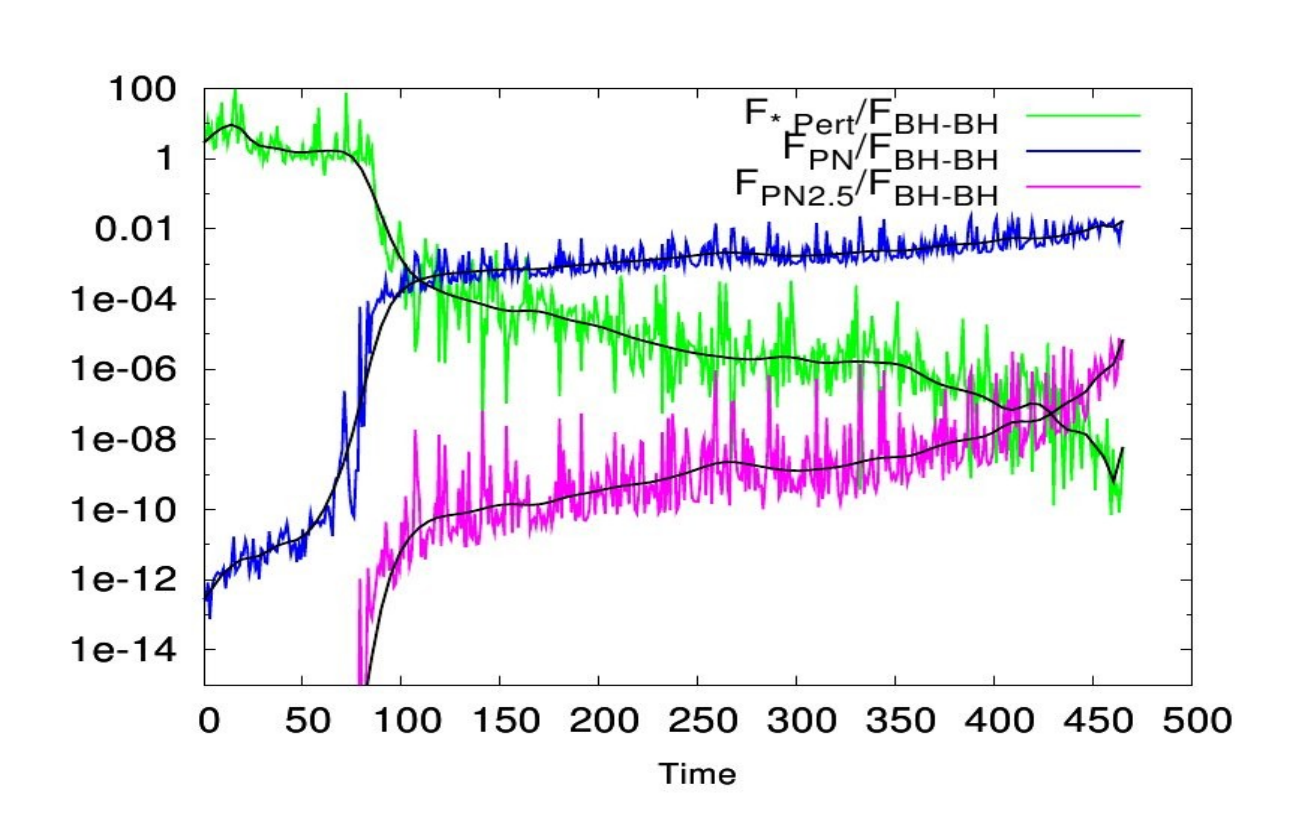

Post-Newtonian Dynamics

Brem, Amaro-Seoane, Spurzem, 2013

Include
Spin-Orbit
Spin-Spin
PN3, PN3.5
Spin Dynamics

By Patrick Brem (Diploma Thesis Univ. Heidelberg)

1PN
2PN + 1.5PN SO
3PN + 2.5PN SO
2.5PN + 2PN SS
3.5PN

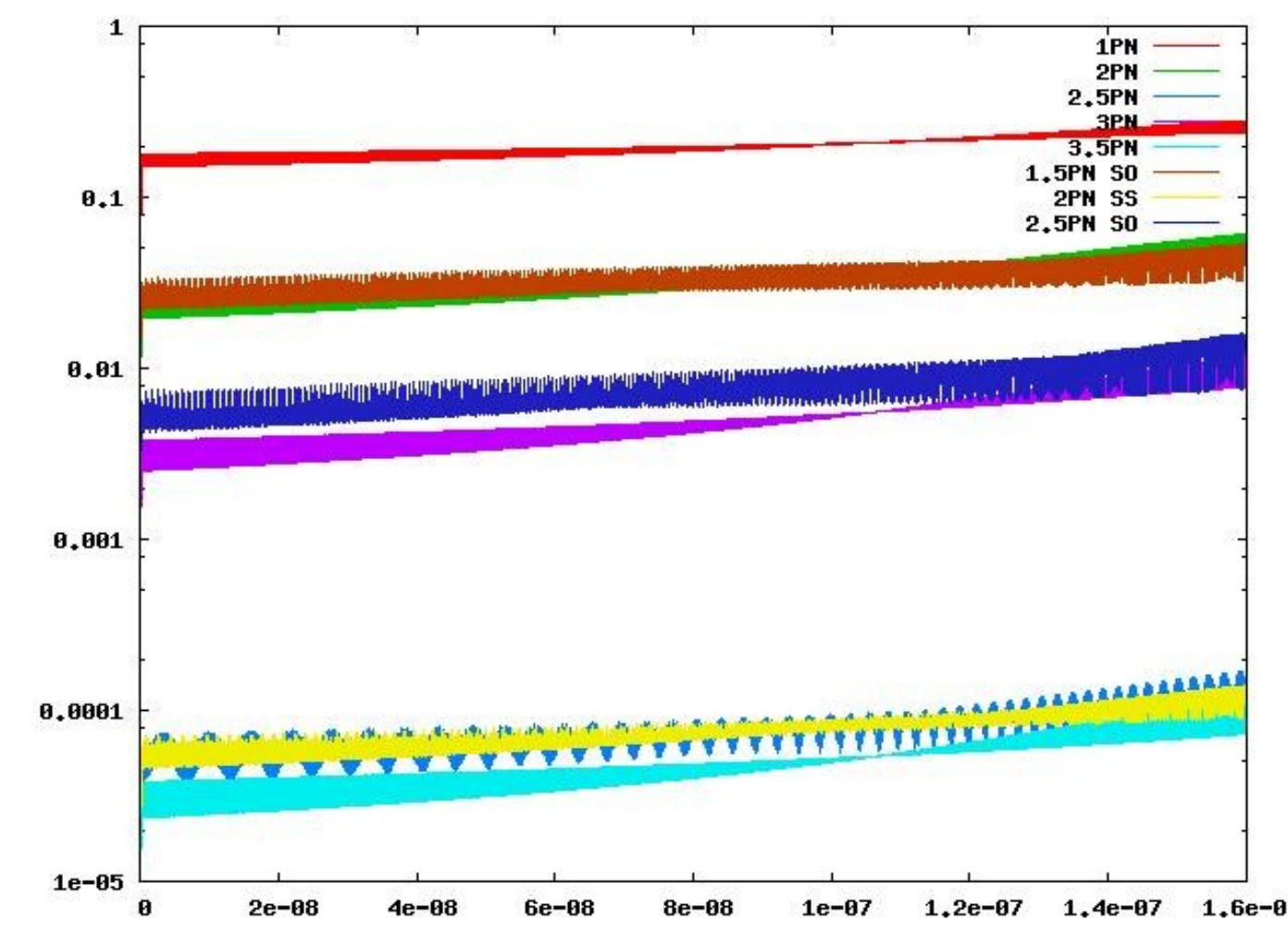

$$|\mathbf{a}_{\rm fin}| = \frac{1}{(1+q)^2}\left[|\mathbf{a}_1|^2 + |\mathbf{a}_2|^2 q^4 + 2|\mathbf{a}_2||\mathbf{a}_1| q^2 \cos\alpha + 2(|\mathbf{a}_1|\cos\beta + |\mathbf{a}_2| q^2 \cos\gamma)|\mathbf{l}| q + |\mathbf{l}|^2 q^2\right]^{1/2},$$

where $q = M_2/M_1$ is the mass ratio and the angles are defined as

$$\cos\alpha = \hat{a}_1 \cdot \hat{a}_2, \qquad \cos\beta = \hat{a}_1 \cdot \hat{l}, \qquad \cos\gamma = \hat{a}_2 \cdot \hat{l}.$$

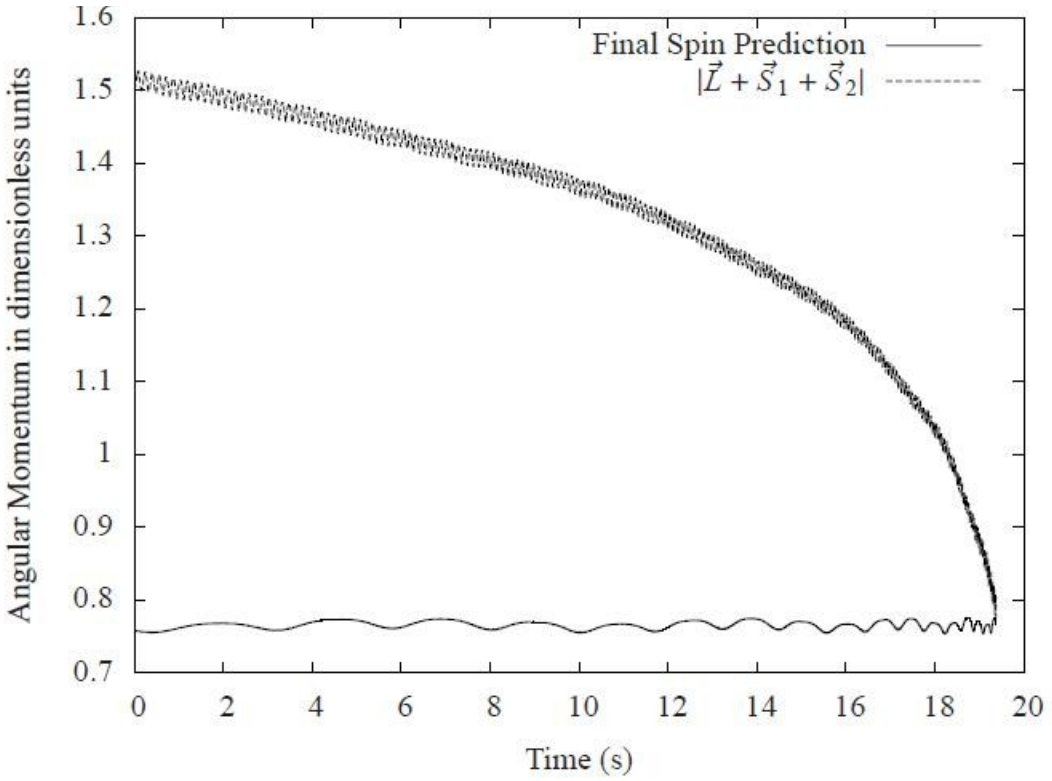

Figure 3.7: Comparison between the current final spin prediction and the actual total angular momentum of the binary system.

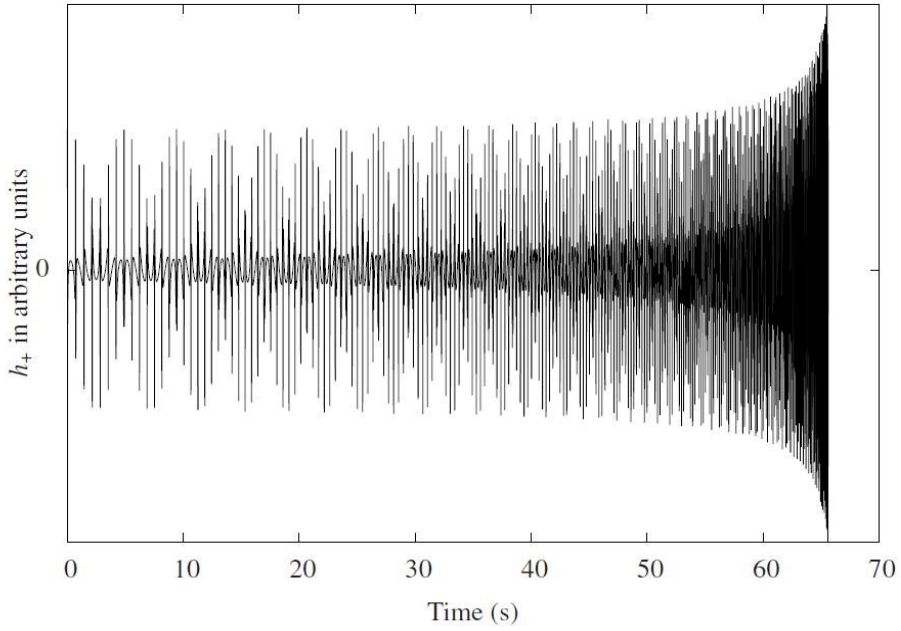

Figure 3.11: Waveform for two equal mass objects on a an orbit with $e = 0.5$.

Post-Newtonian Dynamics Gravitational Wave Templates

Handle spin-orbit and spin-spin coupling (P.Brem, R. Spurzem, Univ. Heidelberg)

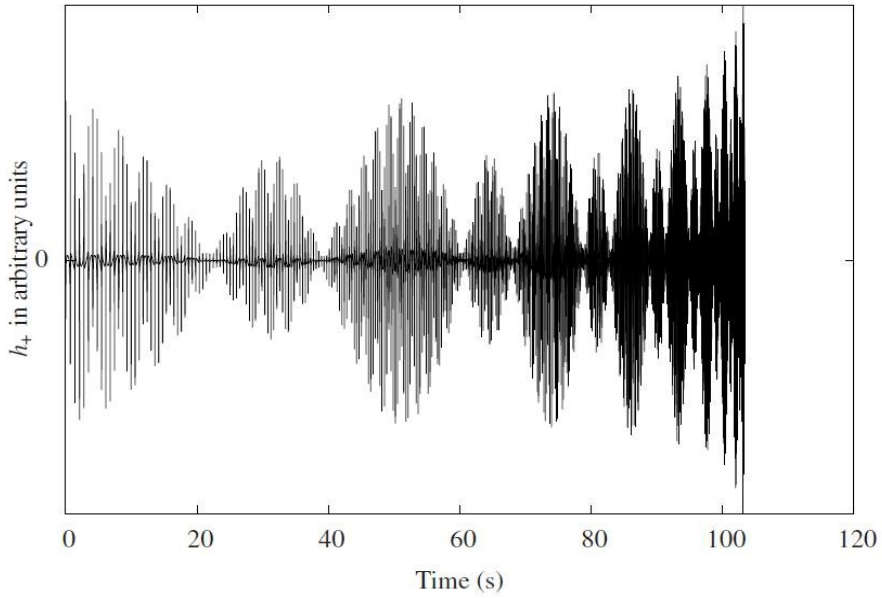

Figure 3.12: Waveform for two objects with a mass ratio of $q = 1/10$ on an orbit with $e = 0.5$ and spins $a_{1,x} = 1.0$, $a_{2,y} = 1.0$.

Brem, Amaro-Seoane, Spurzem, MNRAS, 2013

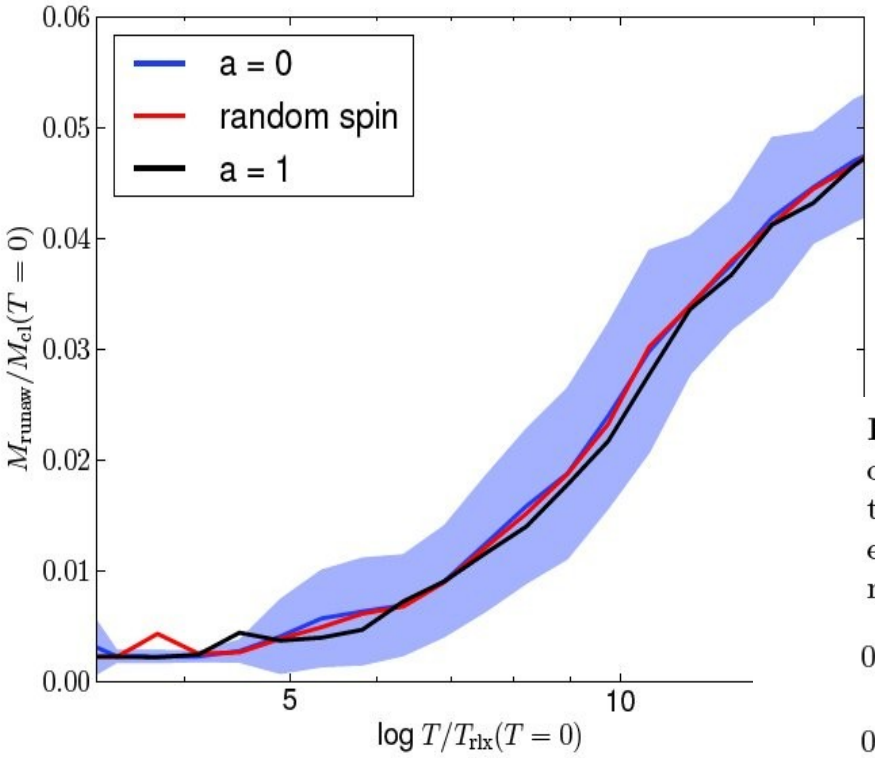

Figure 8. Mass of the runaway body, $M_{\rm runaw}$, for each setup, averaged over 500 runs. $M_{\rm cl}(T=0)$ is the total mass of the cluster at the time $T=0$ and $T_{\rm rlx}(T=0)$ the initial relaxation time of the cluster. The shaded area shows the standard deviation for the $a=0$ case.

Figure 9. Spin of the runaway body in each simulation, averaged over 500 runs. The shaded area shows the standard deviation for the $a=0$ case. All initial spin setups lead to a similar evolution, except for the very first data point which is slightly higher for the maximally spinning initial conditions.

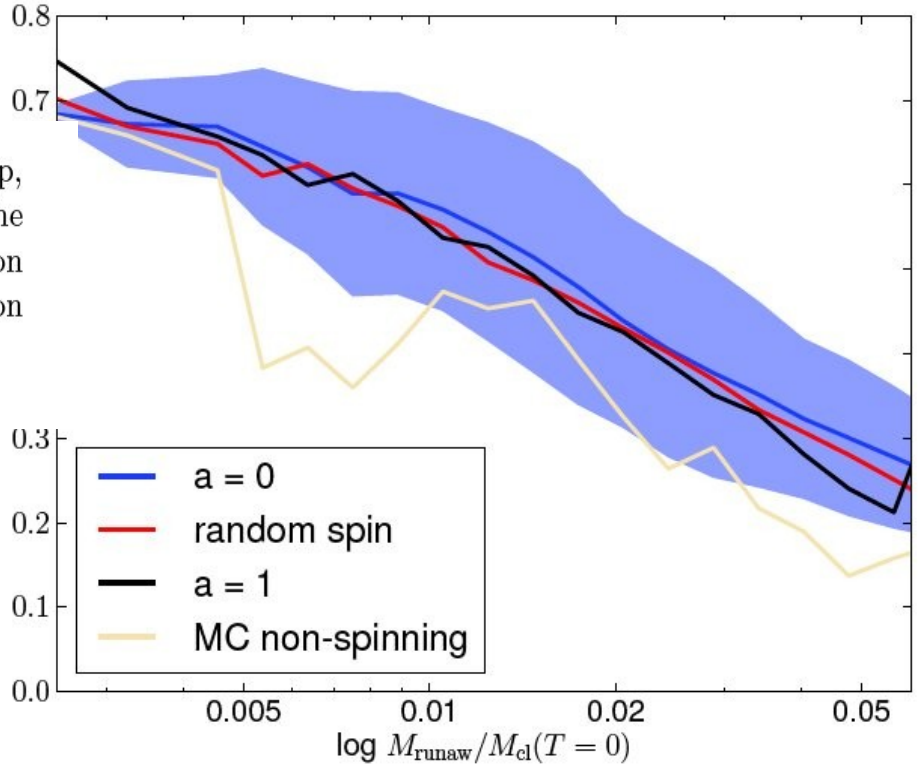

Beij

THE GRAVITATIONAL WAVE SPECTRUM

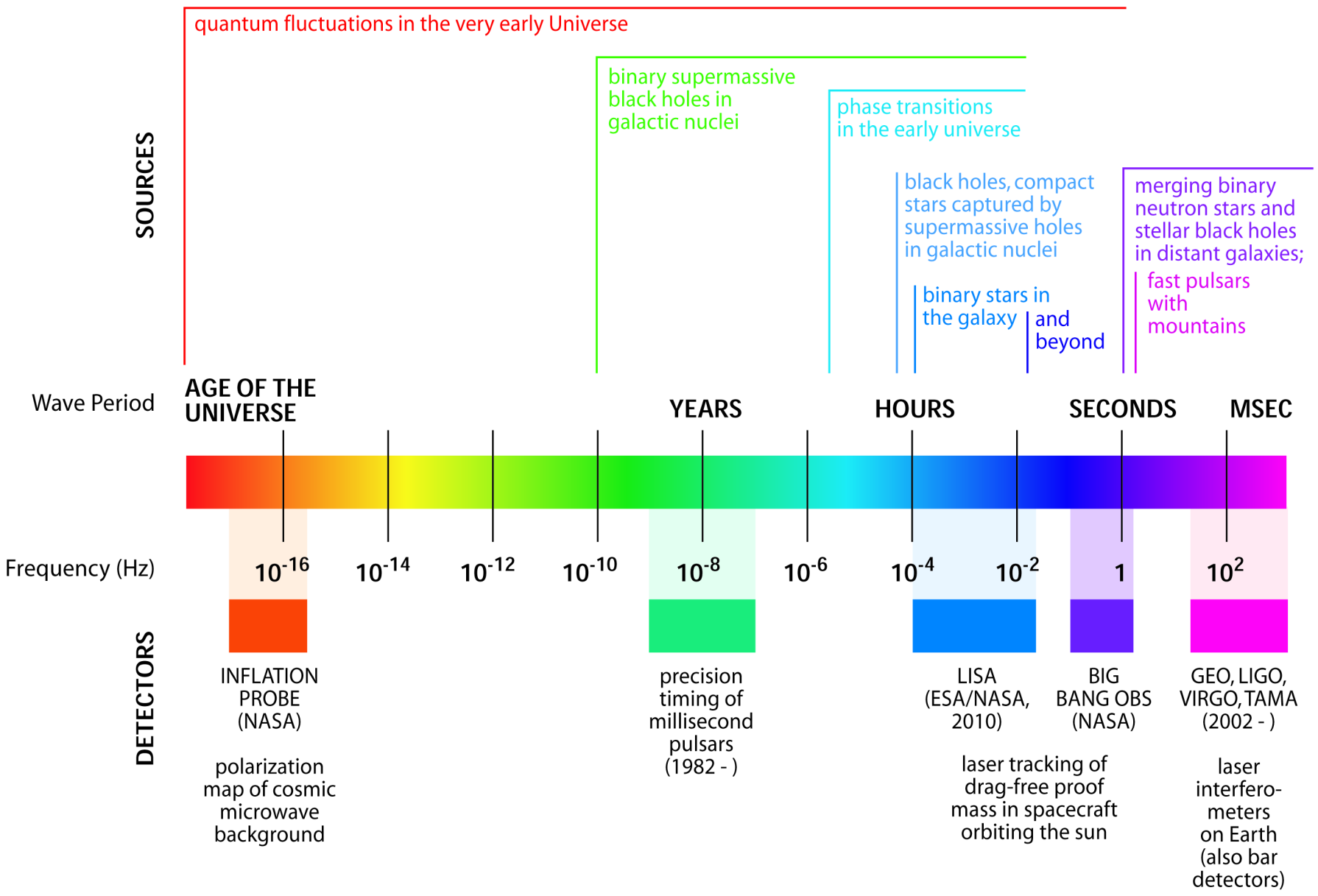

Pulsar Timing

- **Pulsars discovered in Galactic Census also provide network of arms of a huge cosmic gravitational wave detector**
  - **Perturbation in space-time can be detected in timing residuals**
- **Sensitivity: dimensionless strain**

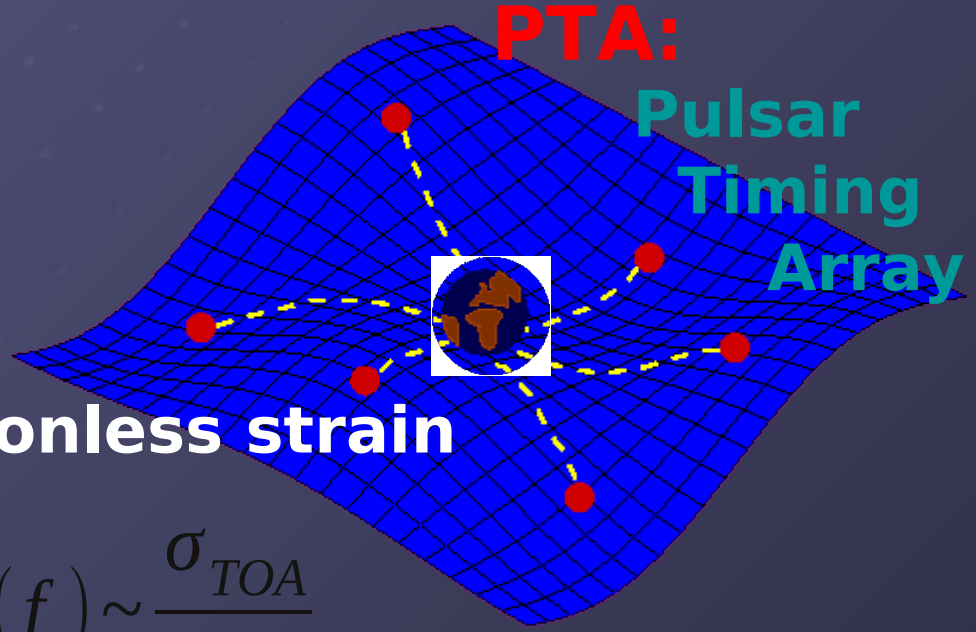

$$h_c(f) \sim \frac{\sigma_{TOA}}{T}$$

Slide by: M. Kramer

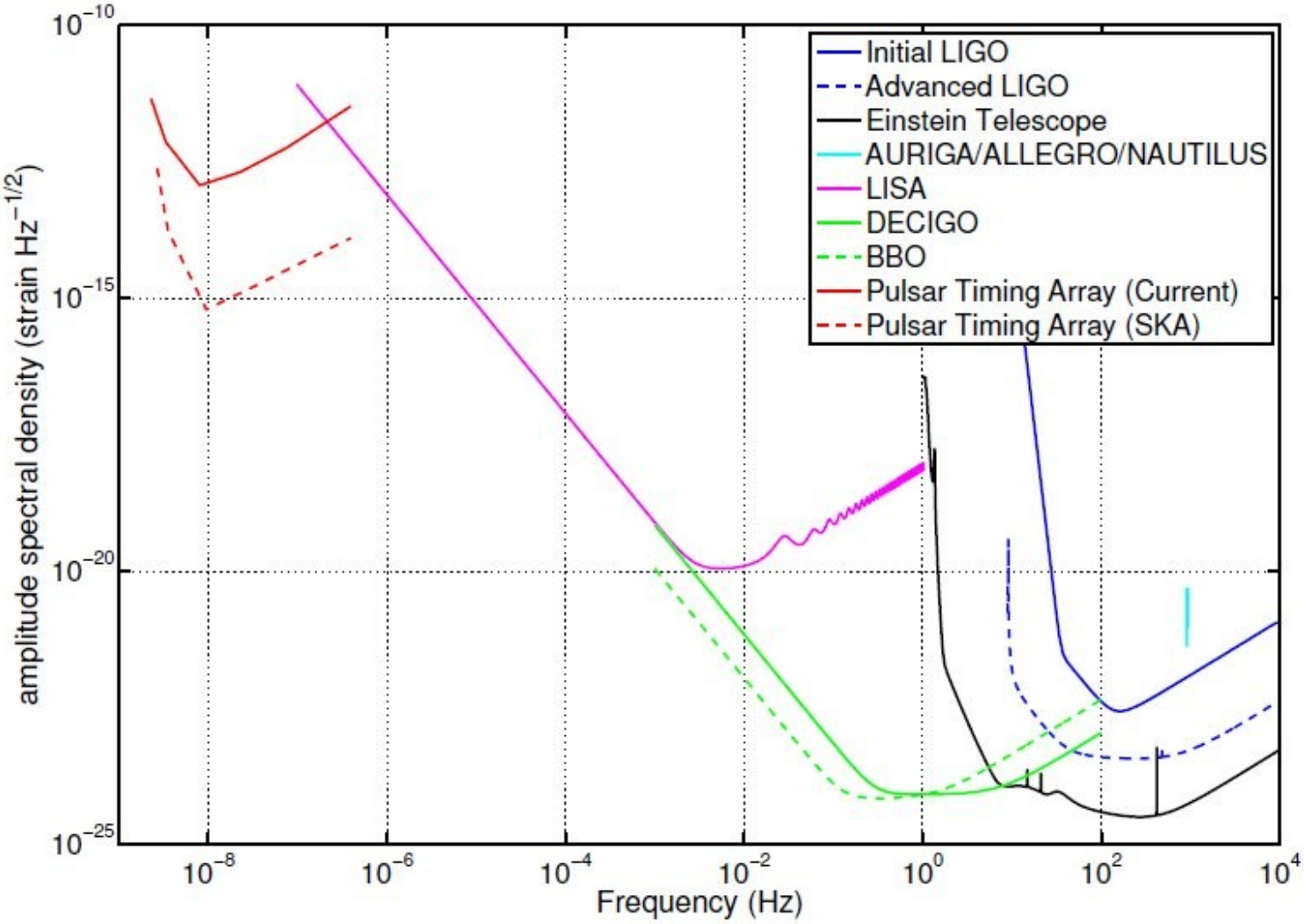

Figure 1: The sensitivity of various gravitational-wave detection techniques across 13 orders of magnitude

From Pitkin et al., Living Reviews 14 (2011) 5, Grav. Wave Detection...

Gravity Waves

current pulsar timing limit ↓

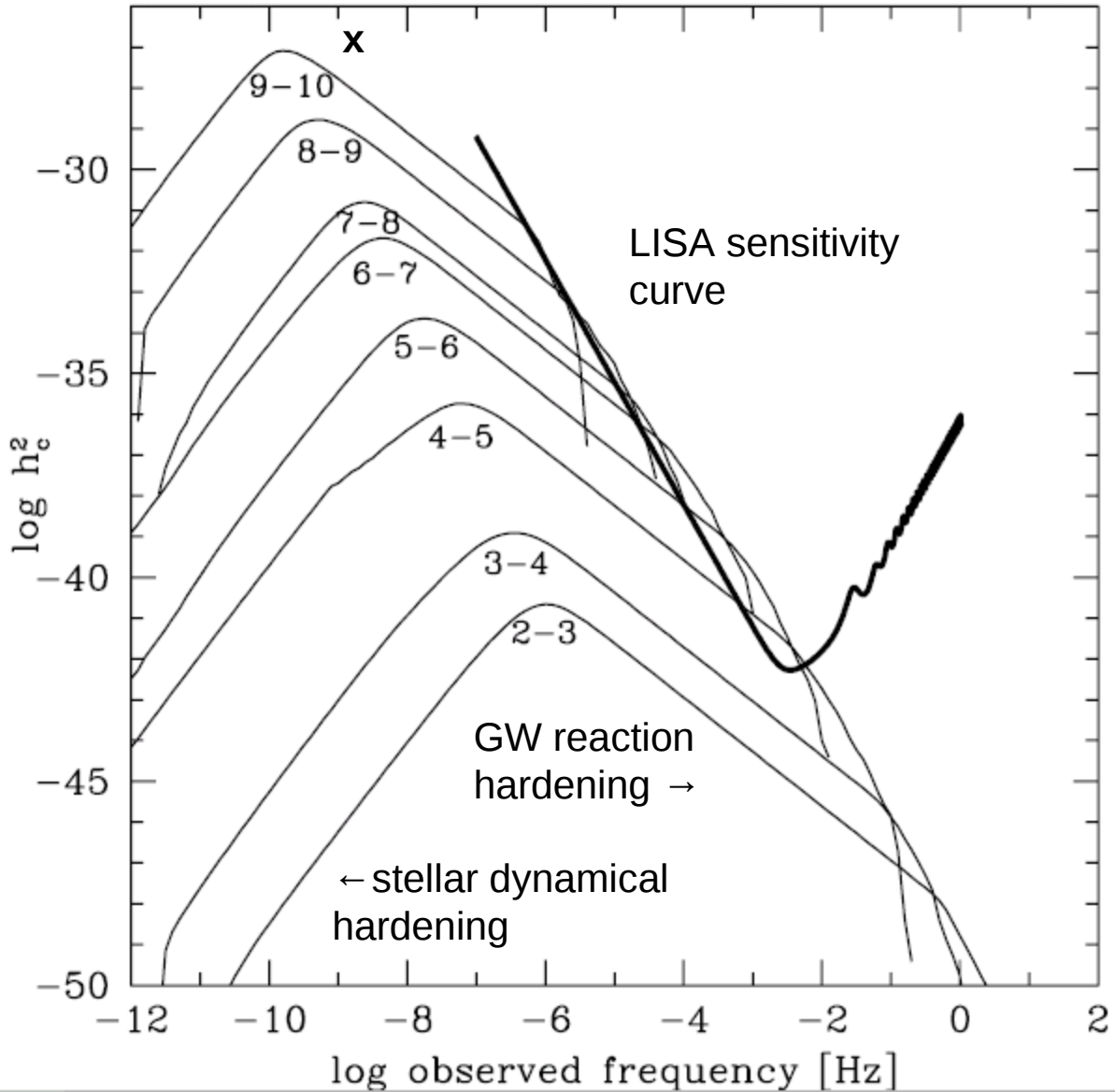

GW background from inspiraling MBH binaries in hierarchical galaxy evolution scenario; square of charact. strain as function of frequency for different black hole masses; current pulsar timing limit indicated: x

NOTE: for this work circular orbits assumed.

From: Sesana, Volonteri, Haardt, Madau 2004 and 2005

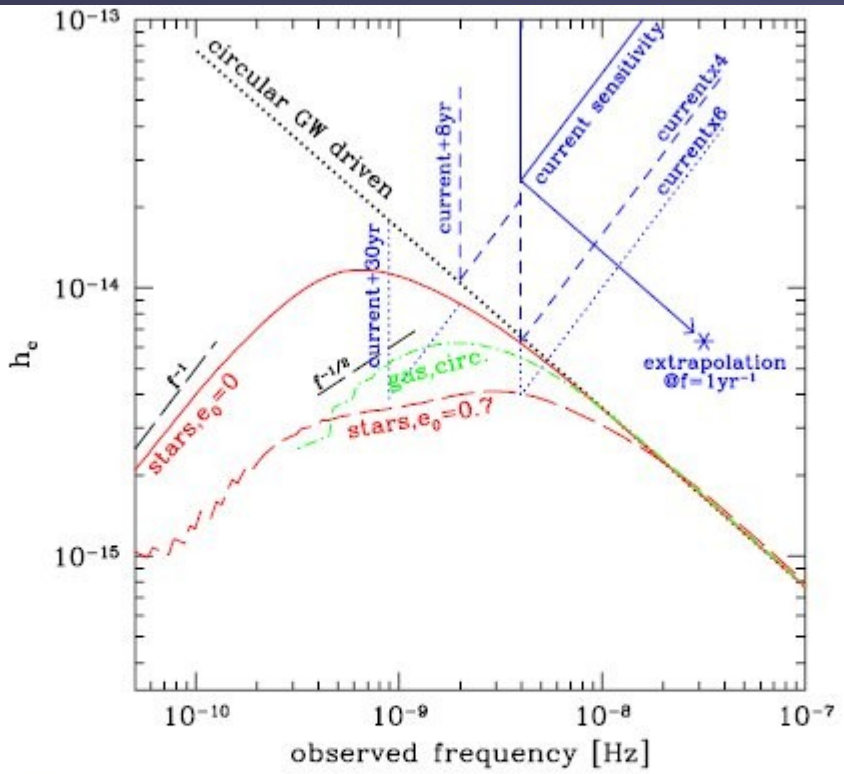

Figure 2. Influence of the binary–environment coupling on the GW signal. The black dotted line denotes the standard $f^{-2/3}$ spectrum for a population of circular GW-driven systems. Red lines are for star-driven binaries with eccentricity of 0 (solid) and 0.7 (long-dashed) at pairing; the green dot–dashed line is for circular gas-driven binaries. A sketch of the current PTA sensitivity is given by the solid blue line, which is then extrapolated to the limit at 1 yr^{-1}. Also shown in blue are extrapolation of the current sensitivity to include 8 and 30 more years of observations (here, we assume no improvement in the timing of the pulsars; the mild improvement in the sensitivity floor is given by the $T^{1/4}$ gain that comes from the longer integration time), as well as the sensitivity given by putative arrays with four and six times better timing precision. We stress that the sensitivity curves are sketchy and only illustrative, but capture the trends relevant to the discussion in the text.

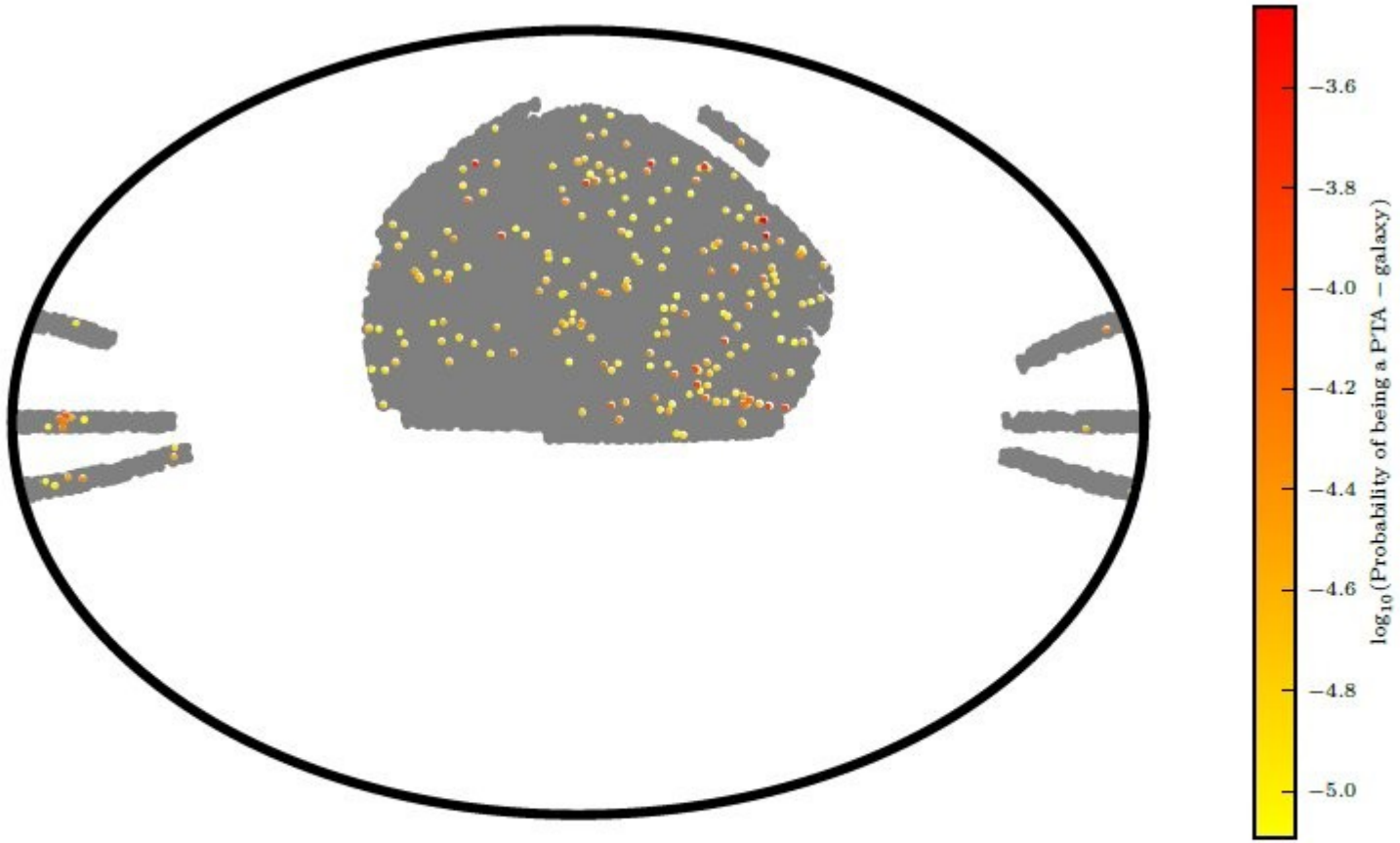

Figure 23. Projected skymap of galaxies from the real catalog (analogous to Figure 20). Now the color bar gives the PTA-galaxy probabilities. Colored points in this plot correspond to real PTA-galaxy candidates, i.e. galaxies that may host a MBHB emitting GWs that produce a maximum strain amplitude larger than $h_0^{\rm thres} = 10^{-15}$. We expect ~ 14 of these 232 candidates to actually be B-galaxies (so they may contain an observable MBHB). The probability of observing one of them is small (as the numbers in the color bar reveal); however, if we do observe a single source from this region of the sky (at $z < 0.1$) with a sensitivity of $h_0^{\rm thres}$, it will most likely be one of these candidates.

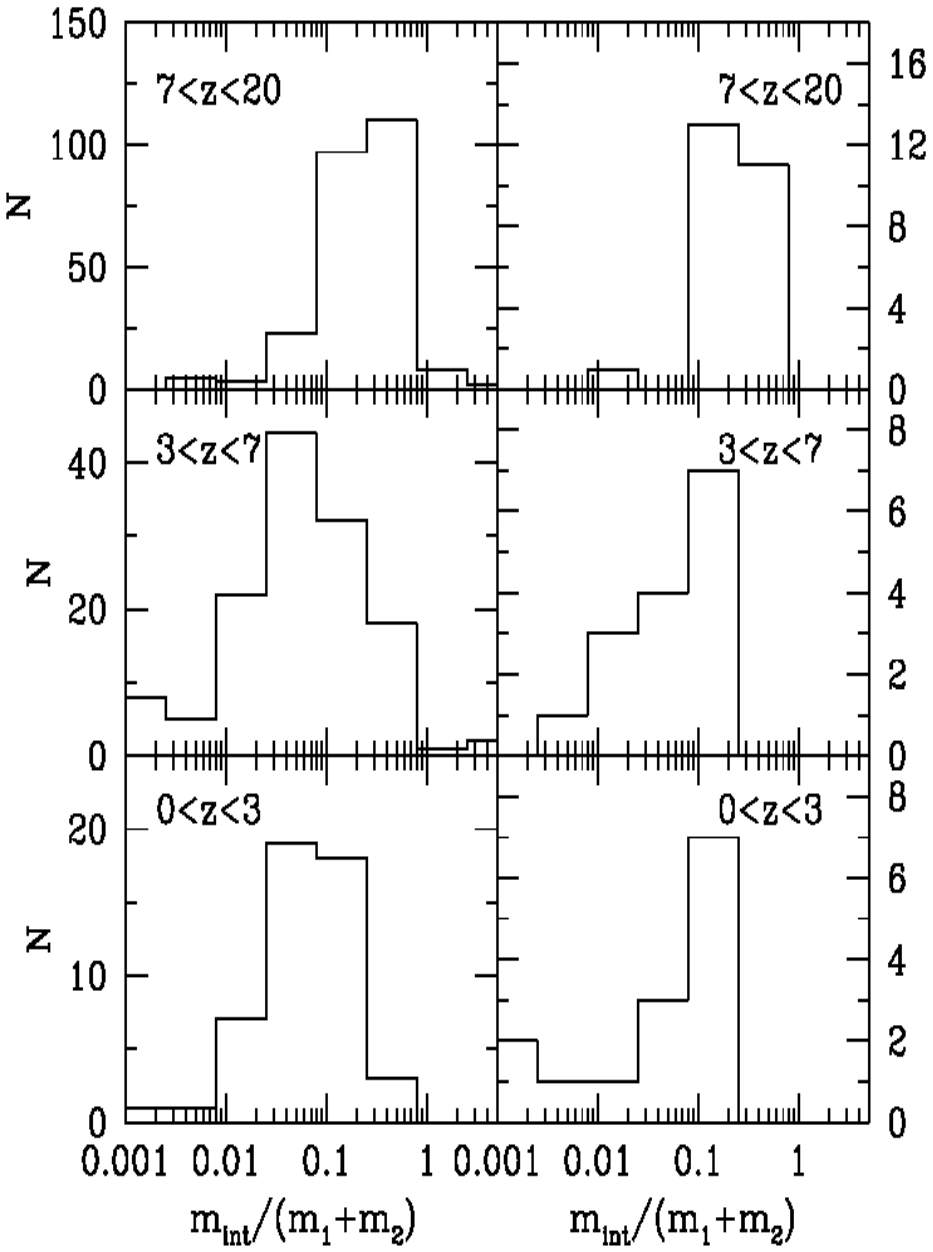

Volonteri et al. 2003

Assumptions:
Every Galaxy has a Black Hole
Simple Ideas for dynamical Friction and Merger timescales Of Binary Black Holes...
...
There are Triple-Black Holes!

FIG. 7.—Number of triple interactions for different ratios between the intruder BH mass $m_{\rm int}$ and the mass $m_1 + m_2$ of the binary, in different redshift intervals. *Left*: $\sigma_{\rm DM} = 250$ km s^{-1}. *Right*: $\sigma_{\rm DM} = 150$ km s^{-1}. This histogram includes results from all 20 Monte Carlo realizations of the same halo mass. At very high redshift (*top panels*, $7 < z < 20$), equal mass system interactions are more common, while at low redshift (*bottom panels*, $0 < z < 3$), a high-mass binary typically interacts with an intruder of much lower mass. At intermediate-high redshift (*middle panels*, $3 < z < 7$), a transition regime occurs.

Galactic Nuclei, Black Holes

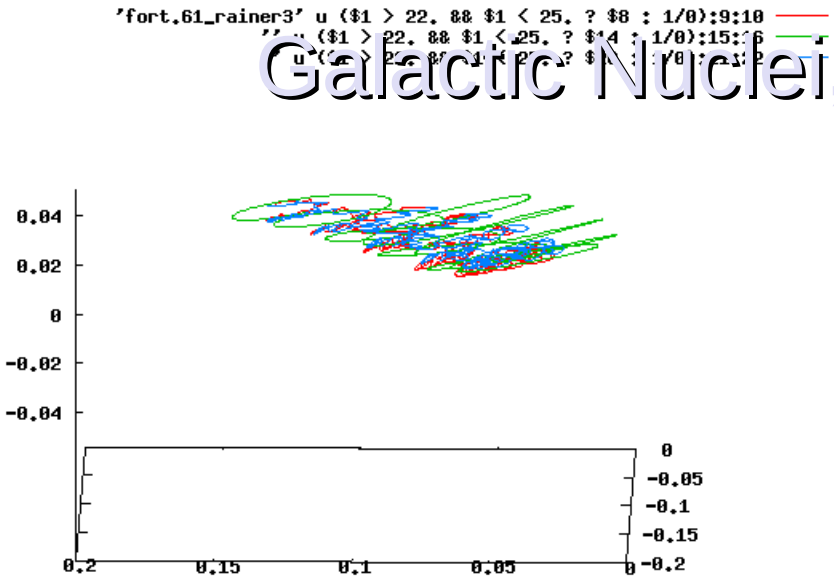

Left: Triple initially coplanar
Bottom: Triple initially nonplanar

We see hierarchical triples,
chaotic three-body,
binary plus single...

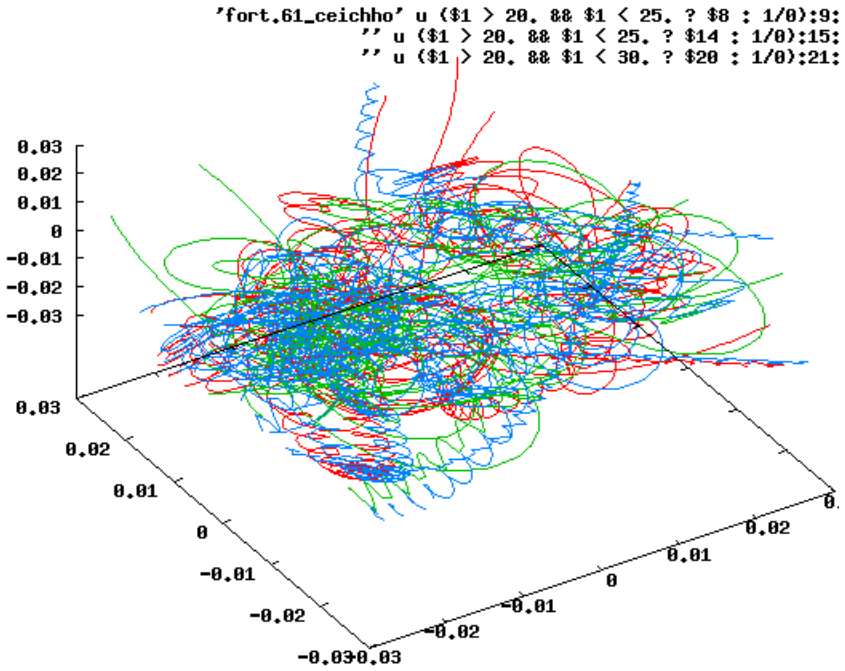

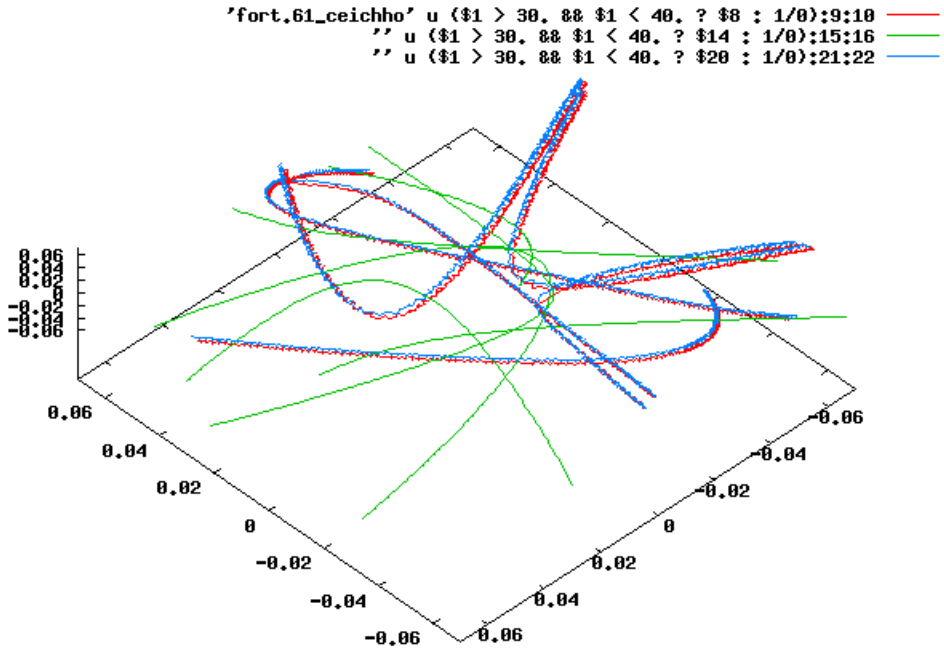

Resonant Triple
Black Hole Dynamics

(Newtonian)

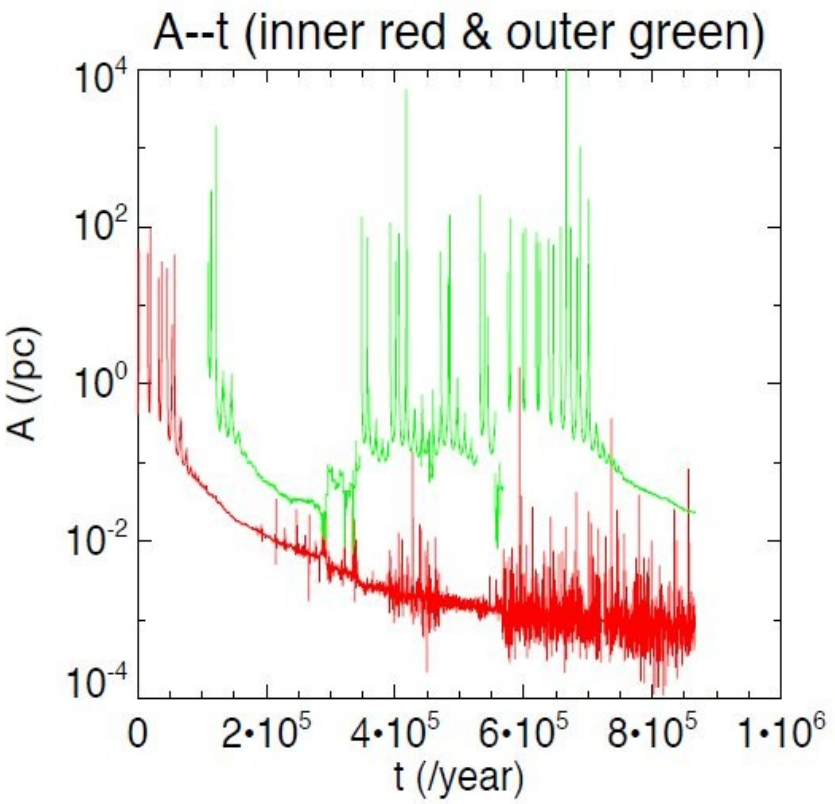

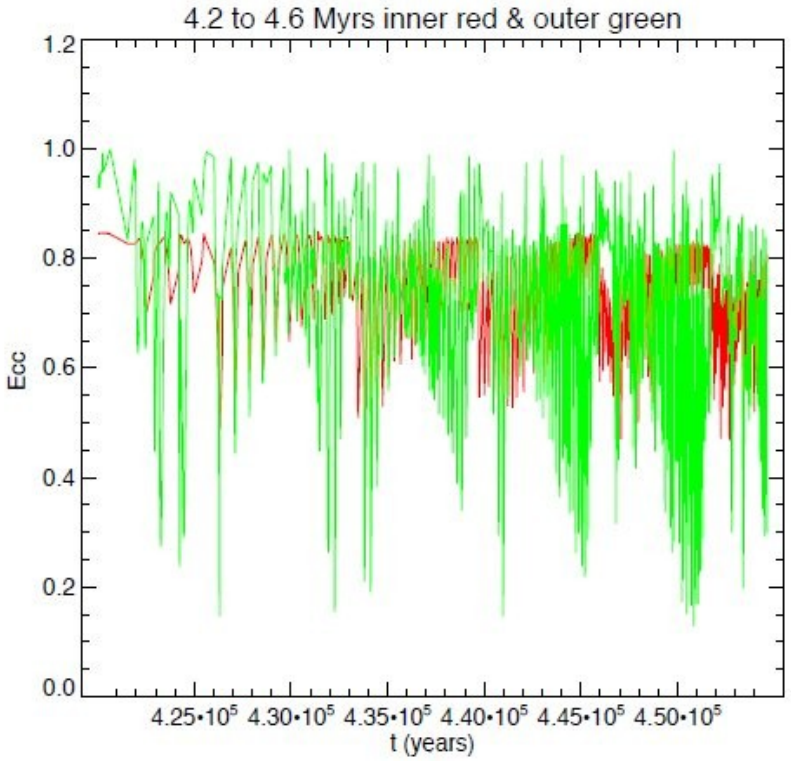

Hao et al. 2014 in prep.

Triplets of supermassive black holes: Astrophysics, Gravitational Waves and Detection:

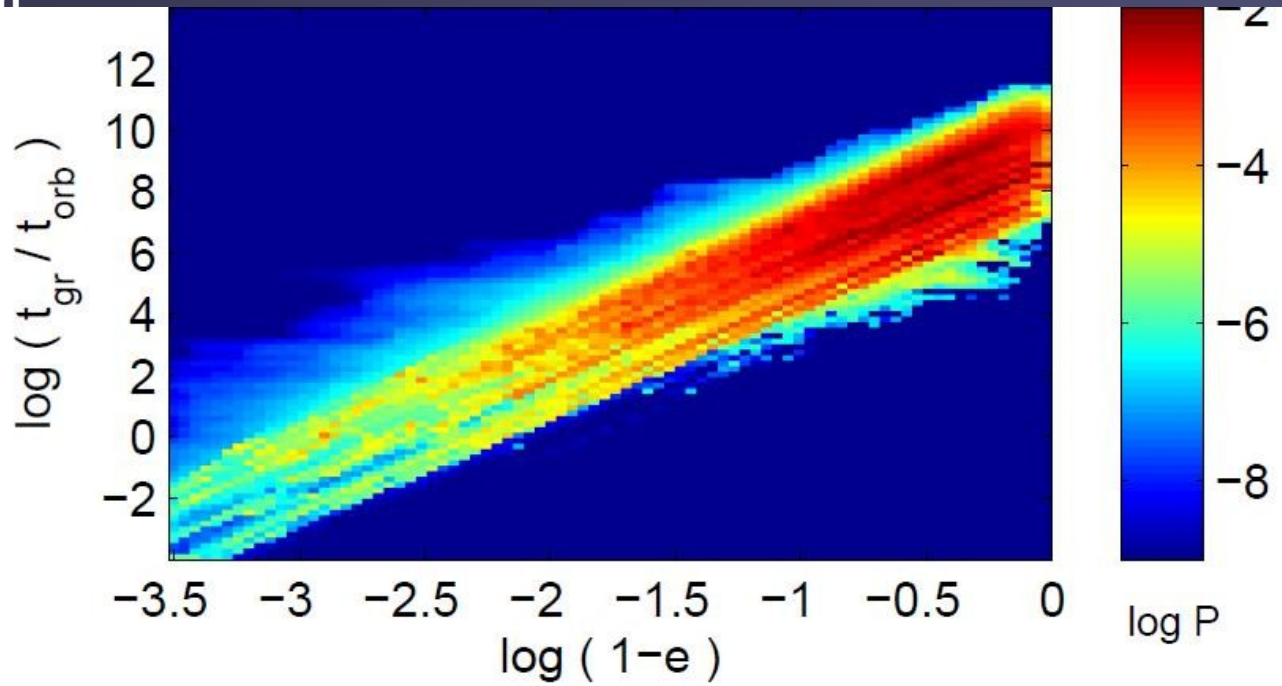

Figure 3. Time spent at different locations in the $t_{\rm gr}$ - (1-e) plane in the Newtonian simulations (blue lines) of Fig. 3. $P := t/t_{\rm close}$ is the probability of finding the binary in a given bin at a randomly chosen time, where $t_{\rm close}$ is the total simulation time spent in close 3-body encounters. The simulation being presented here is the same as the Newtonian simulation (blue lines) in Figure 3. The purpose of this figure is to understand whether gravitational radiation is the main reason for the fall-off in the eccentricity distribution, since the highest eccentricity systems have short coalescence times and quickly disappear. $t_{\rm gr}$ is in years in the upper panel and in orbital periods in the lower panel (the typical resonant encounter takes on order 10^5 yrs). Note that 1-e = 0.002 is about where $t_{\rm gr}$ falls to less than an orbital period

Amaro-Seoane, Sesana, Hoffman, Benacquista, Eichhorn, Makino, Spurzem, MNRAS 402, 2308 (2010)

Triplets of supermassive black holes: Astrophysics, Gravitational Waves and Detection:

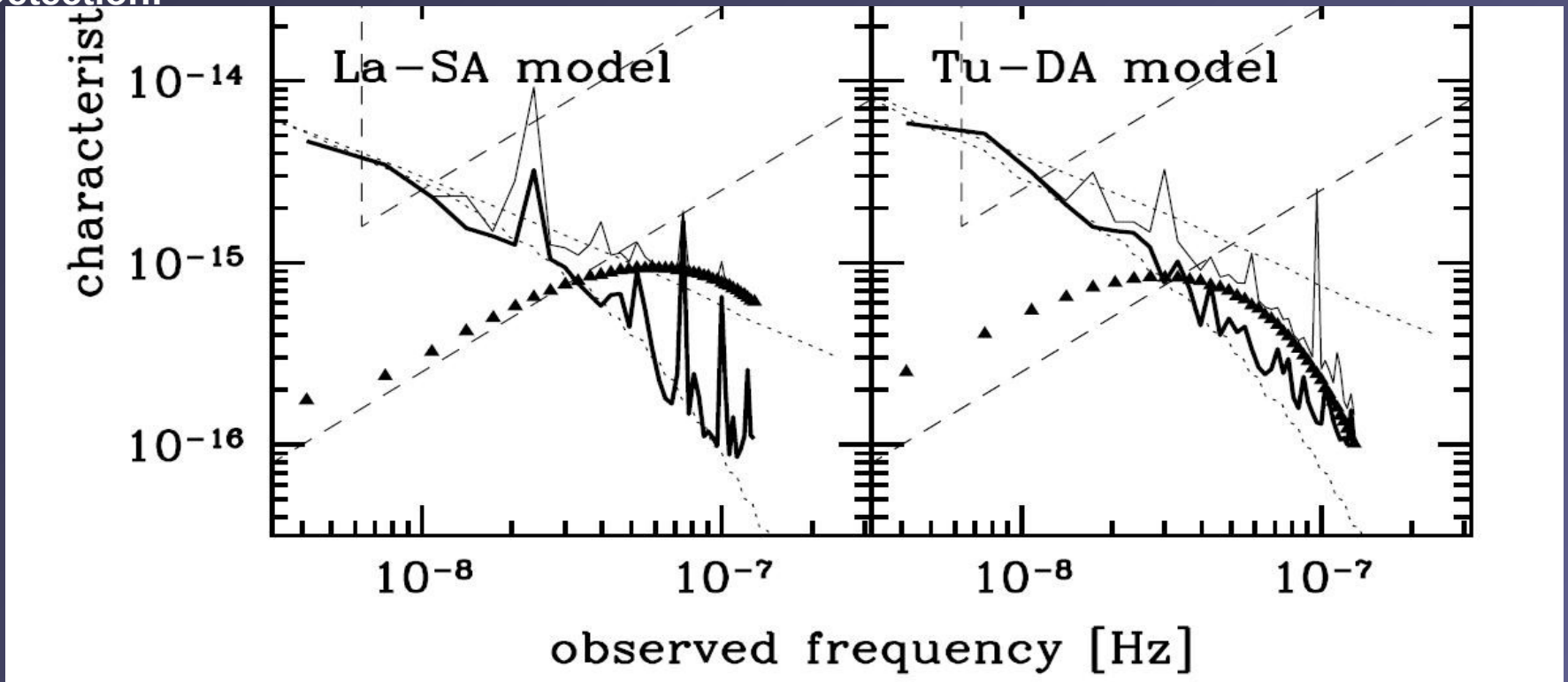

Figure 6. Four examples of GW signals in the PTA window showing potentially detectable features caused by triplet-induced bursts. In each panel, the thin solid line is the total signal, while the thick solid line is the 'unresolved background', which is defined here as the level of the signal once the resolvable events are subtracted. The triangles represent the contribution of a single GW burst to the signal. The two thin dotted lines represent the 'naive' $f^{-2/3}$ background (upper curve) and the actual average confusion noise level (lower curve). The two sets of thin dashed lines represent the expected sensitivity of future PTA campaigns: the complete PPTA (upper curve) and the SKA (lower curve).

Amaro-Seoane, Sesana, Hoffman, Benacquista, Eichhorn, Makino, Spurzem, MNRAS 402, 2308 (2010)

Summary

Gravitational Wave Sources: Time Varying Quadrupole Moment
Binary Black Holes / Neutron Stars
Asymmetric Collapse of Supernova Cores

Current Observation Technique: Laser Interferometry
Ground Based High Frequency (1-1000 Hz)
Space Based Low Frequency (future?)

Pulsar Timing Arrays (ultra low frequency)

Indirect: Binary Pulsars, Supernovae

Multi-Messenger Observations (future): GW observation triggers EM
GW = gravitational wave
EM = electromagnetic